Quantitative Investigation of Compartmentalized Dynamics of ErbB2 Targeting Gold Nanorods in Live Cells by Single Molecule Spectroscopy

Jiji Chen and Joseph Irudayaraj*

Department of Agricultural and Biological Engineering, Bindley Bioscience Center, Purdue Cancer Center and Birck Nanotechnology Center, Purdue University, West Lafayette, Indiana 47907

ABSTRACT Understanding the diffusion dynamics and receptor uptake mechanism of nanoparticles in cancer cells is crucial to the rational design of multifunctional nanoprobes for targeting and delivery. In this report, for the first time, we quantify the localization and evaluate the diffusion times of Herceptin-conjugated gold nanorods (H-GNRs) in different cell organelles by fluorescence correlation spectroscopy (FCS) and examine the endocytic diffusion of H-GNRs in live ErbB2 overexpressing SK-BR-3 cells. First, by colocalizing H-GNRs in different cellular organelles depicted by the respective markers, we demonstrate that H-GNRs colocalize with the endosome and lysosome but not with the Golgi apparatus. Our study shows that Herceptin-conjugated GNRs have similar intracellular localization characteristics as Herceptin—ErbB2 complex, with a higher concentration found in the endosome (72 ± 20.6 nM) than lysosome (9.4 ± 4.2 nM) after internalization. The demonstrated approach and findings not only lay the foundations for a quantitative understanding of the fate of nanoparticle-based targeting but also provide new insights into the rational design of nanoparticle delivery systems for effective treatment.

KEYWORDS: endocytosis · Herceptin—gold nanorods · fluorescence correlation spectroscopy · ErbB2 · quantification · compartmentalization

Studies related to diffusion and uptake of nanoparticles in living cancer cells are rapidly gaining interest because of their potential to serve as intracellular sensors,[1] cancer therapy agents,[2,3] and drug/gene delivery vectors.[4] Endocytic trafficking of targeted nanoparticles involving receptor-mediated internalization, transport, and subsequent breakdown inside living cells is a complex and dynamic process. Understanding the diffusion dynamics and receptor uptake mechanisms of nanoparticles and nanocarriers in cancer cells at single particle level is crucial for effective design of multifunctional nanostructures for imaging, targeting, and therapy.

Recent advances in understanding endocytic mechanisms have used quantum dots (QDs) and nanoparticle-based approaches to study localization, cellular uptake, and intracellular fate;[5−7] however, no report has provided a quantitative assessment of nanoparticle distribution and dynamics at the organelle level in live single cells. Although QDs provide improved photostability, the greater challenge is the cytotoxicity due to the release of heavy metal ions and the complexity in functionalizing, which limits its application in single molecule experiments.[8−10] Gold nanorods (GNRs) have become an attractive alternative because of the ease in control of its size, shape, composition, structure, optical tunability, and nontoxicity to mammalian cells.[11−15] Boyd *et al.*[16] reported that a high level of photon luminescence could be observed from roughened gold metals compared to smooth surfaces by single photon and two photon induced luminescence, and the fluorescence emission of GNRs is millions of times higher than that of bulk gold.[17] Although enhanced single photon and multiphoton luminescence of GNRs was observed years ago, studies were limited to the use of gold nanoparticles as probes for fluorescence imaging.[18−20] We explore for the first time the use of GNRs as fluorescence probes to quantify organelle-specific dynamics in mammalian cells.

In our work, Herceptin, an FDA approved recombinant humanized antibody which binds to the extracellular domain of ErbB2 receptor for the treatment of ErbB2-overexpressing breast cancer,[21] will be used as a targeting ligand. Although several recent advances have reported the use of nanoparticle-conjugated Herceptin constructs as drug targeting and delivery agents for cancer therapy,[22−25] no information is available on quantitative assessment of intracellular diffusion dynamics.

Fluorescence correlation spectroscopy (FCS) allows for the noninvasive *in vivo*

*Address correspondence to josephi@purdue.edu.

Received for review July 5, 2009 and accepted November 2, 2009.

Published online November 5, 2009. 10.1021/nn900743v

monitoring of average residence time (τ_D) and absolute quantification of fluorescing/luminescing probes in a confocal volume at single particle sensitivity. In this research, FCS will be used to investigate the intracellular fate of GNRs and determine its accumulation in different organelles by monitoring the localization of nanoprobes after internalization. Functionalized GNRs with Herceptin (H-GNRs) were used as targeting probes for tracking ErbB2 endocytosis after binding and internalization in live cells. Colocalization of H-GNRs in different cellular organelles was ascertained using appropriate subcellular markers, and the respective diffusion times in the cell membrane, endosome, lysosome, and cytoplasmic compartment were calculated using autocorrelation functions. Our experiments indicate that H-GNRs colocalize with endosome and lysosome but not with the Golgi apparatus. Experiments further indicated that H-GNRs localize in the endosome to a greater extent than the lysosome, and a small amount of H-GNRs escape from the endolysosomal pathway to the cytoplasmic compartments. These quantitative evaluations were made by direct measurement of the absolute concentration of H-GNRs in living cells using live single cell FCS.

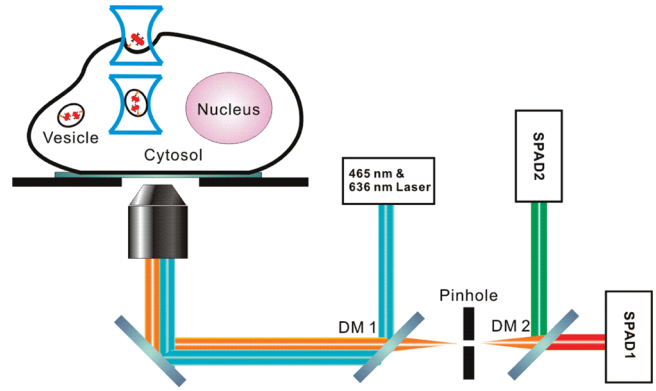

Figure 1. Schematic representation of single point FCS focus on an organelle of interest to investigate the concentration and dynamics of H-GNRs. DM: dichroic mirror. SPAD: single photon avalanche photodiode.

RESULTS AND DISCUSSION

Fluorescence of GNRs. GNRs produced by seed-mediated growth method have a cationic surfactant, cetyltrimethylammonium bromide (CTAB), bound to their surfaces in the form of a bilayer which is known to be cytotoxic and not suitable for live cell studies. For covalent attachment, surface modification of GNRs is essential because the tightly packed CTAB bilayer at the side faces is not easily replaceable for further biofunctionalization.[26,27] In our work, the CTAB bilayer of GNRs was completely replaced with amine groups following the procedure established in our lab[22] and further functionalized with Herceptin (Genentech, San Francisco, CA) targeting the ErbB2 receptor. The amine-modified GNRs have a weak transverse plasmon band at 524 nm and a strong longitudinal plasmon (LP) band at 748 nm, as determined from the UV−visible−NIR spectra (Jasco, Inc., Easton, MD). After Herceptin (H-GNRs) conjugation, the LP peak of the absorption spectra was found to red shift to 758 nm to represent an increase in the local refractive index due to antibody attachment (see Supporting Information, Figure S1). Amine modification of the CTAB capping (by replacement) was confirmed by Fourier transform infrared spectroscopy (FTIR) (Supporting Information, Figure S3). The spectrum for CTAB in the as-prepared substrates shows two intense bands, assigned to asymmetric (2920 cm^{-1}) and symmetric (2850 cm^{-1}) stretching vibrations of $C-CH_2$ in the methylene chains. After amine modification, the intense bands at 2920 and 2850 cm^{-1} become weak, indicating that the CTAB molecules surrounding the gold nanorods have been replaced with amine groups. In addition, quantitative assessment of the amount of antibodies conjugated to a GNR was assessed by collecting the supernatant after centrifuging at 10 000 rpm for 10 min and determining the concentration using the extinction coefficients of Herceptin (protein absorbance maxima ε_{280nm} = 225 000 M^{-1} cm^{-1}).[28] The amount of antibody conjugated to GNR was calculated using the following formula: protein bound to gold nanorods = total protein added − protein in the supernatant solution. The concentration of GNR was estimated using a molar extinction coefficient of 4.4 × 10^9 M^{-1} cm^{-1} at the GNR plasmon resonance wavelength maximum of 730 nm.[14] The number of Herceptin attached to a single gold nanorod was estimated as 89 ± 13 based on the measured concentration of Herceptin and GNRs. The emission maximum of GNRs (aspect ratio ~3.2) as measured by a fluorescence spectrophotometer (Cary Eclipse, Varian, USA) when excited by a 636 nm source was 737 nm (Figure 2a), consistent with the past work.[29] The fluorescence intensity fluctuation count rate (CR) trace of GNRs in real time using two different excitation laser wavelengths (Figure 2b) shows that GNRs with an aspect ratio of 3.2 yield a relatively high fluorescence (14.6 kHz) when excited by the red laser (636 nm) with a 650 nm long pass emission filter and weak signal (0.9 kHz) when excited by the blue laser (465 nm) with 500−540 nm (band-pass) emission filter for similar laser power. Hence, the near-IR emission and the intrinsic fluorescence and the non-photo-bleaching property make GNRs an excellent contrast agent for live cell imaging, interrogation of localization, and dynamics, in the spectral window where biological tissue exhibits relatively small extinction coefficients.

Typical autocorrelation curve of GNRs shown in Figure 5a fitted with two components (eq 2) shows a slow component with a diffusion time of 2.9 ms and a faster

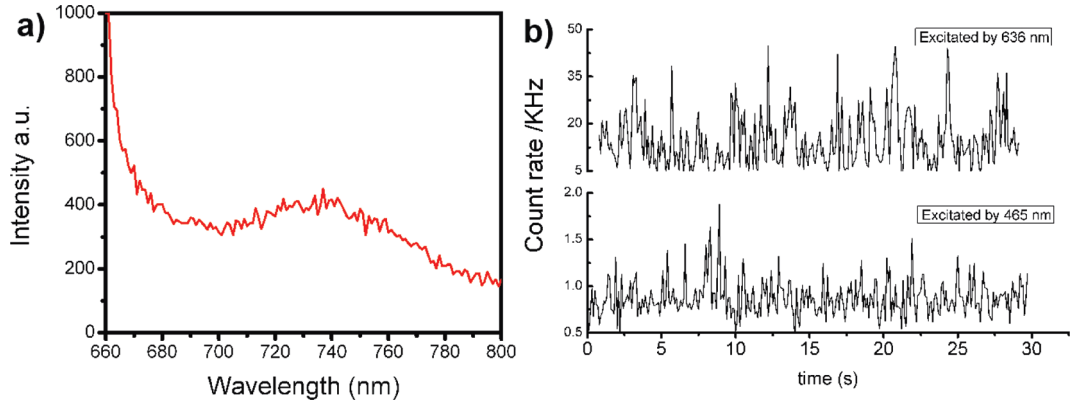

Figure 2. (a) Fluorescence emission spectrum of GNRs with an aspect ratio of 3.2 excited by the 636 nm laser. (b) Fluorescence fluctuation traces of GNRs excited by 636 nm (top) and 465 nm (bottom).

component with a diffusion time of 7 μs with the respective average diffusion coefficients of 7.7×10^{-8} and 3.2×10^{-5} cm^{-2}/s. The diffusion coefficient D is given by $D = \omega^2/4\tau_D$, where ω is the radius of the laser beam size and τ_D the diffusion time. Since the fast diffusion component is even faster than pure fluorescence dyes (*e.g.*, Atto 655), the possibility of small molecule diffusion in the focal volume could be ruled out. We attribute the fast diffusers to the rotational motion of GNRs and the slower component to the average dwelling time as GNRs move in and out of the focal volume. In addition to diffusion, the size of the particles can also be back calculated to confirm the estimations according to Stokes−Einstein equation $D = kT/(6\pi\eta\gamma)$, where k is the Boltzmann constant, T is the temperature, η is the viscosity of liquid, and γ the radius. From calculations, the average hydrodynamic diameter of diffusing GNRs was estimated to be 62 nm, which is in good agreement with the average size (longitudinal average size is 60 ± 4 nm) measured by transmission electron microscopy (TEM) (see Supporting Information, Figure S2). It should be noted that the Stokes−Einstein law is only applicable to spherical particles, and our estimate of the average hydrodynamic diameter of cylindrical rods is only an approximation using the spherical assumption.

Live Cell Imaging Using H-GNRs as Probes. The cytotoxic behavior of amine-modified H-GNRs on SK-BR-3 cells was examined by the MTT (3-(4,5-dimethylthiazol-2-yl)-2,5-diphenyltetrazolium bromide) assay. As expected, the amine-modified GNRs were reasonably nontoxic and biocompatible, while Herceptin-modified GNRs show a dose-dependent toxicity since Herceptin induces apoptosis of breast cancer cells, as shown in Supporting Information, Figure S4. Autofluorescence is often considered as a major problem in single photon excitation FCS at wavelength ranges below 500 nm because flavoproteins, collagen, and elastin are intrinsically fluorescent, and their fluorescence is detectable with the same filter set used for fluorescence imaging in this visible region.[30] Therefore, by exciting GNRs at the red laser wavelength (636 nm), one can minimize interference by autofluorescence. Autocorrelation curve of autofluorescence from bare SK-BR-3 excited by 636 nm laser further confirms that the autofluorescence and consequently the background noise is negligible (Figure S5 of Supporting Information). In addition, by choosing appropriate fluorescence organelle markers, such as yellow fluorescence protein (YFP)-labeled endosome and Golgi in our experiments, we expect to visualize colocalization of H-GNRs in different cellular organelles to quantitatively study their compartmentalized dynamics and intracellular trafficking when internalized through the ErbB2 receptor-mediated endocytosis (Figure 1).

The discrete bright spots (Figure 3b, top) in the cytoplasm of SK-BR-3 cells are indicative of the increased uptake of H-GNRs compared to unmodified GNRs (Figure 3b, bottom) through ErbB2 receptor (overexpressed in SK-BR-3)-mediated endocytosis. Only autofluorescence was observed when GNRs and H-GNR-treated cells were excited by the 465 nm laser (Figure 3a). It is worth noting that ErbB2 receptor-mediated endocyto-

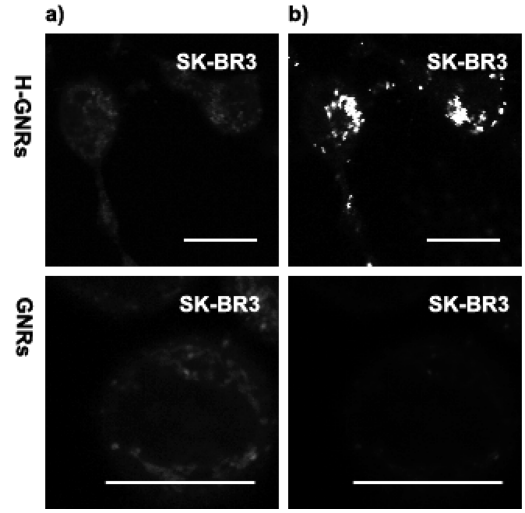

Figure 3. Fluorescence images of H-GNRs (top) and GNRs (down) uptaken by SK-BR-3 cells excited with a 465 nm (a) and 636 nm (b) laser. Scale bars = 15 μm.

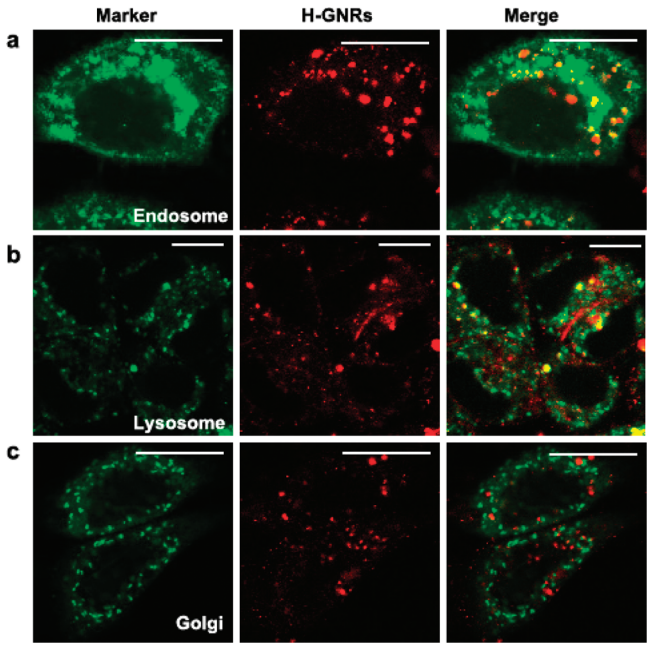

Figure 4. Confocal images of subcellular localization of H-GNRs. SK-BR-3 cells were (a) transfected with RhoB-YFP, (b) stained with LysoTracker green (in green), and (c) transfected with Golgi-YFP and then incubated with H-GNRs (in red). Overlapping signals in merged images appear yellow, the point of focus for FCS data acquisition. Scale bars = 13 μm.

sis occurs very fast, even as early as 30 min post-incubation.

Subcellular localization and dynamics of H-GNRs in different cellular organelles such as Golgi, lysosome, and endosome were monitored using the respective markers. RhoB, which predominantly localizes in the early endosome and recycling endosome,[31] was utilized as an endosomal marker. Since GNRs are excited by the 636 nm laser, the yellow color in the image indicates colocalization with the endosomal markers (Figure 4a). We expect a certain number of H-GNRs to undergo exocytosis by the recycling endosome since RhoB is also a recycling endosomal marker.[32] From the images in Figure 4b, accumulation of H-GNRs was also noted in the lysosome. Internalized H-GNRs did not colocalize with the Golgi marker, suggesting that H-GNRs did not reach this apparatus (Figure 4c). Colocalizing nanoparticles with different fluorescence markers can only provide a qualitative evaluation of this accumulation because of the diffraction-limited optics of confocal imaging. Since the yellow positions show colocalization of GNRs with different cell organelle markers, these locations will be interrogated through point FCS for a quantitative assessment of H-GNR localization in live cells.

Compartmentalized Dynamics of H-GNRs by Single Molecule Spectroscopy. Using single point FCS, the stability of H-GNRs inside living cells was evaluated at different pH. At pH values between 5.0 and 7.4, the autocorrelation curve did not show any significant change in amplitude and the diffusion time was close to the diffusion time of single GNRs, signifying that the GNRs were in a nonaggregated state (data not shown). This information suggests that the probes might be stable even when residing in acidic compartments (with pH = 5.0) such as the endosome and lysosome.[33]

FCS measurements on living membranes could be an intricate procedure due to the low mobility of membrane that could potentially result in photobleaching of fluorescently tagged molecules.[34] Although total internal reflection fluorescence microscopy has predominantly been used to examine cell membranes,[35] in our work, we show elegant autocorrelation curves demonstrating H-GNR dynamics on the cell surface (Figure 5b) fitted with two components using eq 4. The faster component with a diffusion time of 3.5 ± 0.8 ms represents freely diffusing H-GNRs that do not bind to ErbB2. The slower components with a diffusion time of 52 ± 11 ms represent H-GNRs bound to ErbB2 on the cell membrane (Figure 5c). In a few instances, freely diffusing H-GNRs with a diffusion time of 5 ms was found inside cells with an autocorrelation amplitude ($G(0)$, at time $\tau = 0$) in the cytoplasm greater than 1, showing single GNRs mobility in the cytosolic space.

FCS measurement of H-GNR diffusing in different organelles was obtained to determine the accumulation and diffusion dynamics, respectively, in the endosome and lysosome using the respective markers as focus points. Since GNRs do not photobleach, fluorescence measurement was consistent. The autocorrelation curve from the endosome and lysosome was fitted by an anomalous model shown in eq 5 to understand the diffusion characteristics in the cytoplasm,[36,37] which is often crowded by proteins, nucleic acids, and organelles among other constituents. From FCS measurements, the diffusion time of H-GNRs in the endosome and lysosome was calculated to be 12 ± 5 and 20 ± 7 ms, respectively (Figure 5c). On the basis of the diffusion time calculations from FCS and the Stokes−Einstein equation, the corresponding average hydrodynamic diameter of the endosome and lysosome was estimated to be 150 and 280 nm. In these calculations, the viscosity of the fluid phase in the cytosol was approximated to be 1.4 times the viscosity of water.[38] Our calculations of the size estimates of the two cellular organelles matched well with the existing data.[39,40] Although fluorescence correlation spectroscopy (FCS) is a powerful single molecule technique to realize single particle resolution, FCS is effective only when the concentration is kept low (nanomolar) to detect as few as one molecule in a subfemtoliter confocal volume. Hence, in certain cases, this can be a limitation because of the difficulty in controlling the concentration of fluorescent molecules inside live cells and when probing genetically encoded fluorescence protein (*e.g.*, CFP or YFP) expressions or when fluorescently tagged ligands are exogenously introduced into cells. This limitation must be kept in mind when applying FCS for live cell studies.

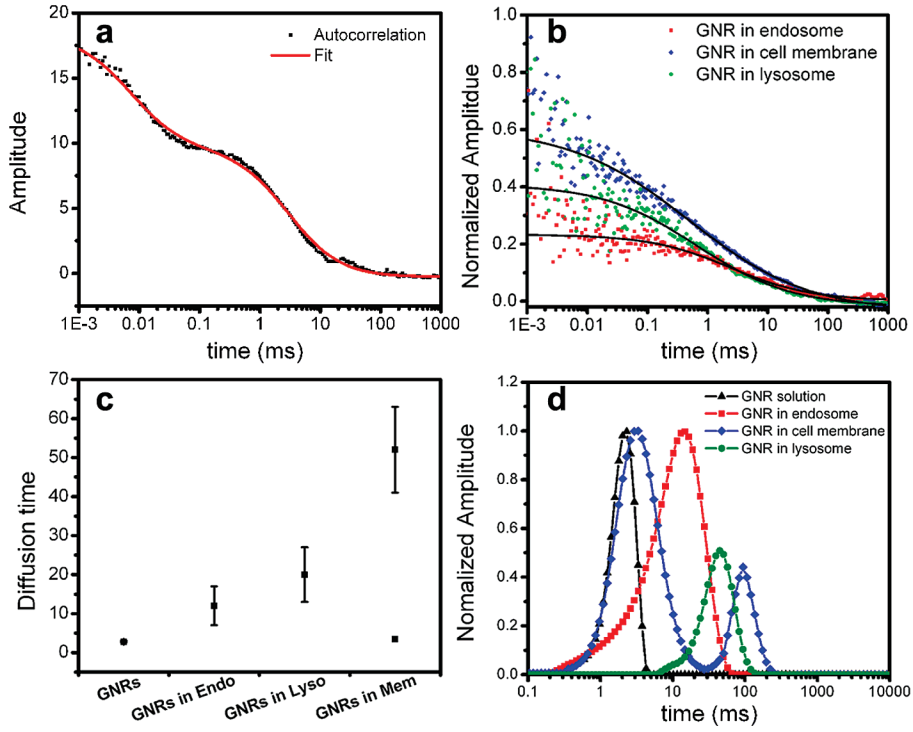

Figure 5. (a) Autocorrelation curve (black dots) of GNRs in solution with an aspect ratio of 3.2 and corresponding curve fitting (red solid line). (b) Autocorrelations of H-GNRs at different measurement positions from cell membrane (■), endosome (●), lysosome (▲), and the corresponding fitted curves (black solid line). (c) Comparison of diffusion time of H-GNRs in solution, endosome, cell membrane, and lysosome by one or two component fitting. (d) Continuous distribution of the diffusion time of H-GNRs in solution, cell membrane, endosome, and lysosome by MEMFCS analysis.

To study the diffusion rates of multiple species, a multicomponent model using the maximum entropy method called MEMFCS[41] was employed to analyze the FCS autocorrelation data (details of MEMFCS are provided in Methods). From MEMFCS, only one peak was noted for the τ_D distribution when monitoring H-GNR diffusion in the endosome and lysosome, as shown in Figure 5d. Here, we observe two peaks corresponding to the distribution of τ_D on the cell membrane to denote unbound components, which follow a faster diffusion time (τ_{D1} peak = 3.2 ms), closer to the diffusion time in solution (2.5 ms) and bound H-GNRs, which corresponds to a slower diffusion time (τ_{D2} peak = 94 ms), consistent with the data fitted to eq 4. In addition, the slowly diffusing H-GNR complexes in the diffusion time range between 50 and 150 ms (Figure 5d) in the cell membrane can be grouped into one cluster, depicting the local environment at the cell membrane or different orders of nanoparticle−receptor complexes at the cell surface in the focal volume. H-GNRs localized in the lysosome showed a slower diffusion time compared to those in the other compartments, possibly due to the organelle-specific confinement and viscosity. Generally, the size of lysosome is bigger than the endosome because it is formed by the fusion of transport vesicles rich in acid hydrolases. In addition, it is found that endosome and lysosome have a more viscous environment than cytosol.[42]

By measuring the amplitude of autocorrelation ($G(0)$, at time $\tau = 0$), the average number of molecules in the detection volume was determined from $G(0) = 1/N = 1/(CV_{eff})$. The concentration ($C$) of H-GNRs at the focus point is estimated from N/V_{eff} by focusing on the cell membrane, endosome, lysosome, and cytosol. Measurements reported in Figure 6 at two different time points are the average from 25 different cells in each category using single point FCS. A significant decrease in the concentration of H-GNRs in the cell membrane ($p < 0.05$) was observed after 6 h, indicating that H-GNRs are efficiently internalized by endocytosis. By contrast, the small increase in the number of H-GNRs observed in

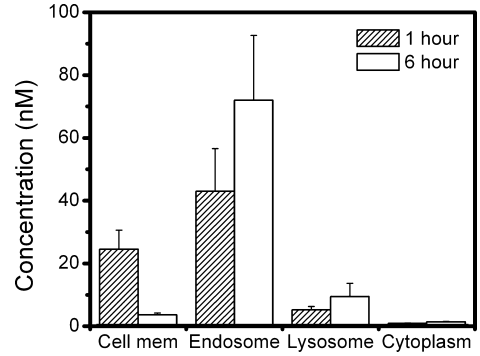

Figure 6. Distribution of H-GNRs in different organelles (cell membrane, endosome, lysosome, and cytosol) at two different time points (1 and 6 h).

the lysosome after 6 h was not significant (ANOVA, $p > 0.05$). In particular, the concentration of H-GNRs in the endosome increased significantly ($p < 0.05$), suggesting that most of the H-GNRs are first trapped in the endosome. Its concentration in the cytoplasm was determined to be 1.4 nM after 6 h, indicating that only a small amount of H-GNRs escaped the endolysosomal pathway to enter the cytoplasm. In the absence of GNRs, although the mechanism of Herceptin intracellular localization is not completely understood, it has been observed that Herceptin does not down-regulate surface ErbB2 but instead efficiently colocalizes in the recycling endosome.[32] By decorating gold nanorods with the Herceptin, our studies found that GNRs did not alter Herceptin distribution characteristics and a predominant accumulation of H-GNRs in the endosome, not the lysosome, which is similar to the past Herceptin−ErbB2 studies.[32] In contrast to previous studies on EGFR trafficking, which showed that EGF could accelerate EGFR internalization followed by efficient lysosome targeting of internalized receptors to result in receptor down-regulation,[43,44] our work demonstrated that H-GNRs−ErbB2 complexes are much less efficient in accumulating in the lysosome and had the same fate as Herceptin−ErbB2.

The above experimental findings suggest a model for ErbB2-mediated endocytosis of the drug-conjugated GNR (H-GNRs), as depicted in Figure 7. We hypothesize that, when H-GNRs are internalized through ErbB2-mediated endocytosis by SK-BR-3 cells, they traffic through the vesicles along microtubules to the sorting endosomal complex. At this stage, an increased numbers of H-GNRs (72 ± 20.6 nM) was found in the endosome, including the sorting and recycling endosome while a lower amount (9.4 ± 4.2 nM) was found to accumulate in the lysosome.

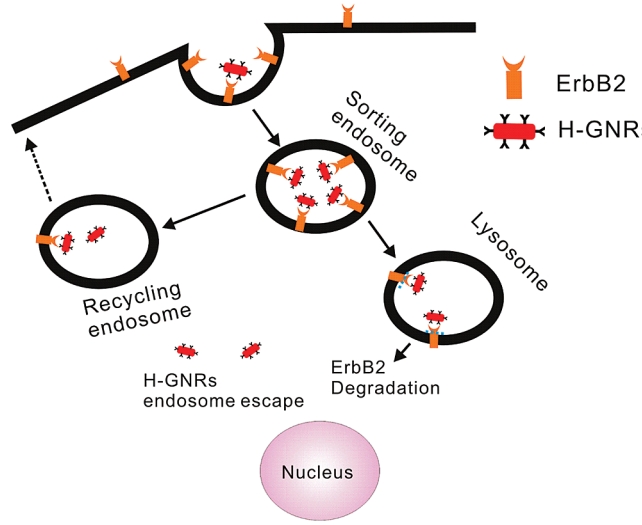

Figure 7. Proposed model of uptake, sorting, and trafficking of H-GNRs through ErbB2 delivery in SK-BR-3 breast cancer cells.

CONCLUSION

In conclusion, we have demonstrated that GNRs could be effectively utilized as fluorescent probes for imaging and more importantly for intracellular trafficking and localization studies using FCS. By colocalizing gold nanorods in different cellular compartments identified by the respective organelle markers, the diffusion times and concentration in the membrane, endosome, and lysosome were assessed. Results indicated that H-GNRs colocalized with the endosome and lysosome but not with the Golgi apparatus. Single molecule experiments using point focus FCS revealed that the concentration of H-GNRs in the endosome was 7.5 times higher than in lysosome. Only a small amount of H-GNRs was found to escape from the endolysosomal pathway to the cytosol, indicating that the therapeutic efficacy of nanoprobes could be enhanced by improving the endosomal escape mechanism. We expect the compartmentalized quantification and dynamics monitoring scheme proposed will help to better understand the intracellular fate of nanoprobes used for therapy and treatment.

METHODS

Cell Organelle Markers and Transient Gene Expression. LysoTracker green (Invitrogen, Carlsbad, CA), YFP-RhoB, and YFP-Golgi were used as lysosome, endosome, and Golgi cellular markers to stain live cells.[45] Cells were transfected using 1 μL Lipofectamine 2000 (Invitrogen, Carlsbad, CA), according to manufacturer's specifications. The amount of DNA used per well in coverslips was 50 ng of YFP-RhoB and YFP-Golgi (YFP-RhoB: YFP coupled to human RhoB GTPase, an enzyme that is localized in early endosomes, recycling endosomes; YFP-Golgi: YFP fusion to residues 1−81 of the β1,4-galactosyltransferase).[45] Five nanomolar LysoTracker probes were added and incubated with cells for 30 min to stain the lysosome in live cells.

Preparation of CTAB-Coated GNRs. Gold nanorods (GNRs) with an aspect ratio of ~3.2 were prepared in aqueous solution using a seed-mediated surfactant-directed method and purified by centrifugation and washing as previously described.[12] Briefly, seed solution was prepared by mixing cetyltrimethylammonium bromide (CTAB) (0.2 M, 5 mL) and $HAuCl_4$ (0.5 mM, 5 mL) with freshly prepared ice-cold $NaBH_4$ (10 mM, 0.6 mL). After 5 h, the seed solution was used for the synthesis of gold nanorods. In a flask, 50.0 mL of 0.2 M CTAB was mixed with 0.3 mL of 4 mM silver nitrate aqueous solution and 50.0 mL of 1 mM $HAuCl_4$. After gently mixing the solution, 700 μL of ascorbic acid (AA) was added. Finally, the seed solution was then added to the growth solution and gently mixed and left undisturbed at room temperature for at least 6 h before use.

Preparation of Amine-Modified GNRs and Antibody Functionalization. Briefly, after preparation of CTAB-stabilized gold nanorods, excess CTAB molecules from 10 mL of gold nanorod solution were removed by centrifuging at 10 000 rpm, and the supernatant was discarded and particles were dispersed in pure water. Then, 1 mL of 30 mM cystamine dihydrochloride was added, and the solution was kept at 60 °C under constant sonication for 3 h. The

resulting GNRs were then collected by centrifuging twice at 7000 rpm for 15 min to remove excess cystamine and CTAB and resuspended in a 0.005 M CTAB solution to yield a final concentration of 100 nM. Herceptin was immobilized to amine-functionalized GNRs using the well-established glutaraldehyde spacer method, and 10 mL of amine-functionalized GNRs was dispersed into 0.01 M phosphate-buffered saline (PBS, NaCl 1.38 M, KCl, 0.0027 M, Tween-20 0.05%, pH 7.4) containing 5% glutaraldehyde for about 1 h. The particles were then collected by centrifugation, redispersed in PBS, and incubated with Herceptin for 12 h at 4 °C. The Herceptin-modified GNRs (H-GNRs) were washed with PBS to remove excess antibodies and kept at 4 °C in pH 7.4 PBS.

Cell Culture and H-GNRs Uptake. SK-BR-3 cells were grown in RPMI-1640 (ATCC) media supplemented with 10% fetal bovine serum. Cells were maintained in an incubator at 37 °C with 5% CO_2. For living-cell fluorescence microscopy studies, cells were seeded onto sterilized No. I coverslip (VWR International, Batavia, IL) and placed inside a 6-well plate. After the cells reached 80% confluence, they were incubated with GNRs or H-GNRs of the same concentration (500 μL, 1 nM) at 37 °C for 1 h and washed with PBS three times. The culture was kept active, and the cells were taken out from the incubator for measurements at different time points (1 and 6 h) when needed.

Confocal Fluorescence Imaging Instrumentation. Fluorescence confocal imaging was performed using scanning confocal time-resolved microscopy (Microtime 200 from Picoquant GmbH, Berlin, Germany); 465 and 636 nm picosecond pulse lasers were employed to excite the cell organelle markers and H-GNRs, respectively. The laser beam was delivered to the sample through an apochromatic 60×, 1.2 NA water immersion objective, and the emitted fluorescence was collected using the same objective and separated from the excitation beam by a dual band dichroic (z467/638rpc, Chroma). A 50 μm pinhole was used to reject the off-focus photons from the excitation volume, and the overall fluorescence was collected and separated accordingly using a dichroic beam splitter (600 dcxr, AHF, Chroma) and filtered by emission filters before being detected by two single photon avalanche photodiodes (SPAD) (SPCM-AQR, PerkinElmer Inc.), as shown in Figure 1. Fluorescence was measured using the time-correlated single photon counting (TCSPC) time-tagged time-resolved (TTTR) mode (Time Harp200, PicoQuant GmbH Berlin, Germany).

Cytotoxicity Experiments. SK-BR-3 cells were seeded in a 96-well plate at a density of 10^4 cells per well in a 100 μL volume. Cells were maintained at 37 °C for 24 h after treatment with H-GNRs and amine-modified GNRs of different concentrations. Cell viability was then determined using an MTT (3-(4,5-dimethylthiazol-2-yl)-2,5-diphenyltetrazolium bromide) assay (MTT Cell Growth Assay Kit, Chemicon, USA). The nanoparticle-treated cells were incubated with the MTT reagent for 4 h (viable cells are capable of metabolizing the MTT reagent, while dead cells are not), and 100 μL of isopropanol with 0.04 N HCl was added to each well and incubated for 30 min, and the absorbance at 570 nm was read. Each concentration was repeated in triplicate, and the results are expressed as percentages.

Data Analysis for FCS. Fluorescence fluctuations of $\delta F(t)$ around the average fluorescence $<F>$ were recorded in real time, and the normalized autocorrelation was calculated as in eq 1.

$$G(\tau) = \frac{<\delta F(t) \times \delta F(t+\tau)>}{<F(t)>^2} \quad (1)$$

where $\delta F(t) = F(t) - <F(t)>$. The autocorrelation curve of GNRs diffusing in solution was fitted to a 3D diffusion model using one or two components with the SymphoTime software (PicoQuant GmbH Berlin, Germany) and Origin Lab using eq 2

$$G(\tau) = \sum \frac{1}{N_i}\left(1 + \frac{\tau}{\tau_{Di}}\right)^{-1}\left(1 + \frac{\tau}{\tau_{Di}\cdot\kappa^2}\right)^{-1/2} \quad (2)$$

N_i and τ_{Di} are the number of fluorescent molecules in the detection volume and diffusion time of component i, respectively; κ is defined as the ratio of the axial beam size z and radius ω of the laser. For calibration of effective confocal volume, aqueous solutions of Rhodamine 123 and Atto 655 dyes (Invitrogen Molecular Probes Eugene, OR) were used. Assuming a 3D Gaussian observation volume approximated by $V_{eff} = \pi^{3/2}\omega^2 z$, a blue laser confocal volume of 0.58 fL was obtained. Similarly, using Atto 655 dye with the 636 nm excitation, a red laser confocal volume of 1.2 fL was obtained.

Since the cytosol is an extremely crowded environment, the simplest model that could accurately describe the autocorrelation data of H-GNR diffusion is the anomalous diffusion model observed in the cytoplasm[36,37] as given by

$$G(\tau) = \frac{1}{N}\cdot\left(1 + \left(\frac{\tau}{\tau_D}\right)^{\alpha}\right)^{-1}\cdot\left(1 + \left(\frac{1}{\kappa^2}\left(\frac{\tau}{\tau_D}\right)^{\alpha}\right)\right)^{-1/2} \quad (3)$$

where α represents the degree of anomalous behavior. Values of α vary from 0.5 to 0.8, consistent with values reported in the literature for live-cell studies.[36,37]

Diffusion of free H-GNRs above the cell surface can be described by the 3D diffusion function, whereas diffusion of bound H-GNRs on the cell membrane can be represented by the 2D diffusion function given by the autocorrelation function given in eq 4 as

$$G(\tau) = \frac{1}{\langle N\rangle}\left((1-y)\left(1 + \frac{\tau}{\tau_d^{free}}\right)^{-1}\left(1 + \frac{\tau}{\tau_d^{free}\cdot\kappa^2}\right)^{-1/2} + y\left(1 + \frac{\tau}{\tau_d^{bound}}\right)^{-1}\right) \quad (4)$$

where τ_d^{free} is the diffusion time of unbound H-GNRs, τ_d^{bound} is the diffusion time of bound H-GNRs, and y is the fraction of bound H-GNRs diffusing at time τ_d^{bound}.

To further validate the autocorrelation data of H-GNR diffusion in live cells, a multicomponent model using the maximum entropy method called MEMFCS[41] was construed. MEMFCS is based on minimizing χ^2 as well as maximizing entropy S to obtain an optimal fit when the diffusion times of the different species are involved in a given focal volume. Thus, $G(\tau)$ in eq 2 can be rewritten to obtain a continuous distribution of diffusion time using MEMFCS as

$$G(\tau) = \int \alpha_i\left(1 + \frac{\tau}{\tau_D}\right)^{-1}\left(1 + \kappa^2\frac{\tau}{\tau_D}\right)^{-1/2} d\tau_D \quad (5)$$

S is defined as

$$S = \sum_i p_i \ln p_i, \quad \text{where } p_i = \alpha_i / \sum \alpha_i \quad (6)$$

Unlike the conventional fitting method, which fits different diffusion components (*i.e.*, 1, 2, 3 *etc.*) given *a priori*, MEMFCS yields a size distribution instead of a discrete value which is particularly attractive and more relevant for the analysis of heterogeneous systems.

Data obtained were expressed as mean ± standard deviation and analyzed by one-way ANOVA with the Post Hoc Tukey's test applied for paired comparisons. A difference between means was considered significant if the p value is less than 0.05.

Acknowledgment. Funding from the Trask grant and the Fellowship for JC from the Office of the Vice President for Research at Purdue University is acknowledged. Professors Maiti and Periaswamy (TIFR, Mumbai) are acknowledged for providing the MEMFCS software. The YFP-Endo and YFP-Golgi constructs were gifts from Dr. C. Berlot (Weis Center for Research, Danville, PA). Dr. Chungang Wang is acknowledged for assistance in gold nanorod synthesis. Herceptin was a generous gift from Genentech Inc. (San Francisco, CA). Finally, the authors thank Dr. Pierre-Alexandre Vidi for the helpful insights.

Supporting Information Available: Figures of UV−vis and FTIR spectra of GNRs, TEM images, cytoxicity of GNRs, and FCS autofluorescence curves are available. This material is available free of charge *via* the Internet at http://pubs.acs.org.

REFERENCES AND NOTES

1. Heller, D. A.; Jeng, E. S.; Yeung, T. K.; Martinez, B. M.; Moll, A. E.; Gastala, J. B.; Strano, M. S. Optical Detection of DNA Conformational Polymorphism on Single-Walled Carbon Nanotubes. *Science* **2006**, *311*, 508–511.
2. Hirsch, L. R.; Stafford, R. J.; Bankson, J. A.; Sershen, S. R.; Rivera, B.; Price, R. E.; Hazle, J. D.; Halas, N. J.; West, J. L. Nanoshell-Mediated Near-Infrared Thermal Therapy of Tumors under Magnetic Resonance Guidance. *Proc. Natl. Acad. Sci. U.S.A.* **2003**, *100*, 13549–13554.
3. El-Sayed, I. H.; Huang, X.; El-Sayed, M. A. Selective Laser Photo-Thermal Therapy of Epithelial Carcinoma Using Anti-EGFR Antibody Conjugated Gold Nanoparticles. *Cancer Lett.* **2006**, *239*, 129–135.
4. Ghosh, P.; Han, G.; De, M.; Kim, C. K.; Rotello, V. M. Gold Nanoparticles in Delivery Applications. *Adv. Drug Delivery Rev.* **2008**, *60*, 1307–1315.
5. Rajan, S. S.; Liu, H. Y.; Vu, T. Q. Ligand-Bound Quantum Dot Probes for Studying the Molecular Scale Dynamics of Receptor Endocytic Trafficking in Live Cells. *ACS Nano* **2008**, *2*, 1153–1166.
6. Barua, S.; Rege, K. Cancer-Cell-Phenotype-Dependent Differential Intracellular Trafficking of Unconjugated Quantum Dots. *Small* **2009**, *5*, 370–376.
7. Ruan, G.; Agrawal, A.; Marcus, A. I.; Nie, S. Imaging and Tracking of Tat Peptide-Conjugated Quantum Dots in Living Cells: New Insights into Nanoparticle Uptake, Intracellular Transport, and Vesicle Shedding. *J. Am. Chem. Soc.* **2007**, *129*, 14759–14766.
8. Jamieson, T.; Bakhshi, R.; Petrova, D.; Pocock, R.; Imani, M.; Seifalian, A. M. Biological Applications of Quantum Dots. *Biomaterials* **2007**, *28*, 4717–4732.
9. Kirchner, C.; Liedl, T.; Kudera, S.; Pellegrino, T.; Javier, A. M.; Gaub, H. E.; Stolzle, S.; Fertig, N.; Parak, W. J. Cytotoxicity of Colloidal CdSe and CdSe/ZnS Nanoparticles, *Nano Lett.* **2005**, *5*, 331–338.
10. Bachir, A. I.; Kolin, D. L.; Heinze, K. G.; Hebert, B.; Wiseman, P. W. a Guide to Accurate Measurement of Diffusion Using Fluorescence Correlation Techniques with Blinking Quantum Dot Nanoparticle Labels. *J. Chem. Phys.* **2008**, *128*, 225105.
11. Jana, N. R.; Gearheart, L.; Murphy, C. J. Wet Chemical Synthesis of High Aspect Ratio Cylindrical Gold Nanorods. *J. Phys. Chem. B* **2001**, *105*, 4065–4067.
12. Nikoobakht, B.; El-Sayed, M. A. Preparation and Growth Mechanism of Gold Nanorods (NRs) Using Seed-Mediated Growth Method. *Chem. Mater.* **2003**, *15*, 1957–1962.
13. Jana, N. R. Gram-Scale Synthesis of Soluble, Near-Monodisperse Gold Nanorods and Other Anisotropic Nanoparticles. *Small* **2005**, *1*, 875–882.
14. Perez-Juste, J.; Pastoriza-Santos, I.; Liz-Marzan, L. M.; Mulvaney, P. Gold Nanorods: Synthesis, Characterization and Applications. *Coord. Chem. Rev.* **2005**, *249*, 1870–1901.
15. Connor, E. E.; Mwamuka, J.; Gole, A.; Murphy, C. J.; Wyatt, M. D. Gold Nanoparticles Are Taken up by Human Cells but Do Not Cause Acute Cytotoxicity. *Small* **2005**, *1*, 325–327.
16. Boyd, G. T.; Yu, Z. H.; Shen, Y. R. Photoinduced Luminescence from the Noble Metals and Its Enhancement on Roughened Surfaces. *Phys. Rev. B* **1986**, *33*, 7923–7936.
17. Mohamed, M. B.; Volkov, V.; Link, S.; El-Sayed, M. A. The 'Lightning' Gold Nanorods: Fluorescence Enhancement of over a Million Compared to the Gold Metal. *Chem. Phys. Lett.* **2000**, 517–523.
18. Durr, N. J.; Larson, T.; Smith, D. K.; Korgel, B. A.; Sokolov, K.; Ben-Yakar, A. Two-Photon Luminescence Imaging of Cancer Cells Using Molecularly Targeted Gold Nanorods. *Nano Lett.* **2007**, *7*, 941–945.
19. Wang, H.; Huff, T. B.; Zweifel, D. A.; He, W.; Low, P. S.; Wei, A.; Cheng, J. X. *In Vitro* and *In Vivo* Two-Photon Luminescence Imaging of Single Gold Nanorods. *Proc. Natl. Acad. Sci. U.S.A.* **2005**, *102*, 15752–15756.
20. He, H.; Xie, C.; Ren, J. Nonbleaching Fluorescence of Gold Nanoparticles and Its Applications in Cancer Cell Imaging. *Anal. Chem.* **2008**, *80*, 5951–5957.
21. Slamon, D. J.; Leyland-Jones, B.; Shak, S.; Fuchs, H.; Paton, V.; Bajamonde, A.; Fleming, T.; Eiermann, W.; Wolter, J.; Pegram, M.; Baselga, J.; Norton, L. Use of Chemotherapy Plus a Monoclonal Antibody against HER2 for Metastatic Breast Cancer That Overexpresses HER2. *N. Engl. J. Med.* **2001**, *344*, 783–792.
22. Wang, C.; Chen, J.; Talavage, T.; Irudayaraj, J. Gold Nanorod/Fe_3O_4 Nanoparticle "Nano-Pearl-Necklaces" for Simultaneous Targeting, Dual-Mode Imaging, and Photothermal Ablation of Cancer Cells. *Angew. Chem., Int. Ed.* **2009**, *48*, 2759–2763.
23. Xu, C.; Wang, B.; Sun, S. Dumbbell-like Au-Fe_3O_4 Nanoparticles for Target-Specific Platin Delivery. *J. Am. Chem. Soc.* **2009**, *131*, 4216–4217.
24. Anhorn, M. G.; Wagner, S.; Kreuter, J.; Langer, K.; von Briesen, H. Specific Targeting of HER2 Overexpressing Breast Cancer Cells with Doxorubicin-Loaded Trastuzumab-Modified Human Serum Albumin Nanoparticles. *Bioconjugate Chem.* **2008**, *19*, 2321–2331.
25. Sun, B.; Ranganathan, B.; Feng, S. S. Multifunctional Poly(D,L-lactide-*co*-glycolide)/Montmorillonite (PLGA/MMT) Nanoparticles Decorated by Trastuzumab for Targeted Chemotherapy of Breast Cancer. *Biomaterials* **2008**, *29*, 475–486.
26. Pierrat, S.; Zins, I.; Breivogel, A.; Sonnichsen, C. Self-Assembly of Small Gold Colloids with Functionalized Gold Nanorods. *Nano Lett* **2007**, *7*, 259–263.
27. Yu, C.; Varghese, L.; Irudayaraj, J. Surface Modification of Cetyltrimethylammonium Bromide-Capped Gold Nanorods to Make Molecular Probes. *Langmuir* **2007**, *23*, 9114–9119.
28. Bhattacharyya, S.; Wang, S.; Reinecke, D.; Kiser, W., Jr.; Kruger, R. A.; DeGrado, T. R. Synthesis and Evaluation of Near-Infrared (NIR) Dye−Herceptin Conjugates as Photoacoustic Computed Tomography (PCT) Probes for HER2 Expression in Breast Cancer. *Bioconjugate Chem.* **2008**, *19*, 1186–1193.
29. Eustis, S.; El-Sayed, M. Aspect Ratio Dependence of the Enhanced Fluorescence Intensity of Gold Nanorods: Experimental and Simulation Study. *J. Phys. Chem. B* **2005**, *109*, 16350–16356.
30. Schwille, P.; Haupts, U.; Maiti, S.; Webb, W. W. Molecular Dynamics in Living Cells Observed by Fluorescence Correlation Spectroscopy with One- and Two-Photon Excitation. *Biophys. J.* **1999**, *77*, 2251–2265.
31. Adamson, P.; Paterson, H. F.; Hall, A. Intracellular-Localization of the P21(Rho) Proteins. *J. Cell Biol.* **1992**, *119*, 617–627.
32. Austin, C. D.; De Maziere, A. M.; Pisacane, P. I.; van Dijk, S. M.; Eigenbrot, C.; Sliwkowski, M. X.; Klumperman, J.; Scheller, R. H. Endocytosis and Sorting of ErbB2 and the Site of Action of Cancer Therapeutics Trastuzumab and Geldanamycin. *Mol. Biol. Cell* **2004**, *15*, 5268–5282.
33. Lee, R. J.; Wang, S.; Low, P. S. Measurement of Endosome pH Following Folate Receptor-Mediated Endocytosis. *Biochim. Biophys. Acta* **1996**, *1312*, 237–242.
34. Adkins, E. M.; Samuvel, D. J.; Fog, J. U.; Eriksen, J.; Jayanthi, L. D.; Vaegter, C. B.; Ramamoorthy, S.; Gether, U. Membrane Mobility and Microdomain Association of the Dopamine Transporter Studied with Fluorescence Correlation Spectroscopy and Fluorescence Recovery after Photobleaching. *Biochemistry* **2007**, *46*, 10484–10497.
35. Yu, C.; Hale, J.; Ritchie, K.; Prasad, N. K.; Irudayaraj, J. Receptor Overexpression or Inhibition Alters Cell Surface Dynamics of EGF−EGFR Interaction: New Insights from Real-Time Single Molecule Analysis. *Biochem. Biophys. Res. Commun.* **2009**, *378*, 376–382.
36. Weiss, M.; Elsner, M.; Kartberg, F.; Nilsson, T. Anomalous Subdiffusion Is a Measure for Cytoplasmic Crowding in Living Cells. *Biophys. J.* **2004**, *87*, 3518–3524.

37. Banks, D. S.; Fradin, C. Anomalous Diffusion of Proteins Due to Molecular Crowding. *Biophys. J.* **2005**, *89*, 2960–2971.
38. Fushimi, K.; Verkman, A. S. Low Viscosity in the Aqueous Domain of Cell Cytoplasm Measured by Picosecond Polarization Microfluorimetry. *J. Cell Biol.* **1991**, *112*, 719–725.
39. Kulkarni, R. P.; Castelino, K.; Majumdar, A.; Fraser, S. E. Intracellular Transport Dynamics of Endosomes Containing DNA Polyplexes along the Microtubule Network. *Biophys. J.* **2006**, *90*, L42–L44.
40. Ganley, I. G.; Carroll, K.; Bittova, L.; Pfeffer, S. Rab9 GTPase Regulates Late Endosome Size and Requires Effector Interaction for Its Stability. *Mol. Biol. Cell* **2004**, *15*, 5420–5430.
41. Sengupta, P.; Garai, K.; Balaji, J.; Periasamy, N.; Maiti, S. Measuring Size Distribution in Highly Heterogeneous Systems with Fluorescence Correlation Spectroscopy. *Biophys. J.* **2003**, *84*, 1977–1984.
42. Yoshida, N.; Kinjo, M.; Tamura, M. Microenvironment of Endosomal Aqueous Phase Investigated by the Mobility of Microparticles Using Fluorescence Correlation Spectroscopy. *Biochem. Biophys. Res. Commun.* **2001**, *280*, 312–318.
43. Sorkin, A.; Von Zastrow, M. Signal Transduction and Endocytosis: Close Encounters of Many Kinds. *Nat. Rev. Mol. Cell Biol.* **2002**, *3*, 600–614.
44. Lidke, D. S.; Nagy, P.; Heintzmann, R.; Arndt-Jovin, D. J.; Post, J. N.; Grecco, H. E.; Jares-Erijman, E. A.; Jovin, T. M. Quantum Dot Ligands Provide New Insights into ErbB/HER Receptor-Mediated Signal Transduction. *Nat. Biotechnol.* **2004**, *22*, 198–203.
45. Vidi, P. A.; Chen, J.; Irudayaraj, J. M.; Watts, V. J. Adenosine A(2A) Receptors Assemble into Higher-Order Oligomers at the Plasma Membrane. *FEBS Lett.* **2008**, *582*, 3985–3990.